

## Article

# Thermal Blooming Effect of Power-Exponent-Phase Vortex Beams Propagating through the Atmosphere

Feng Zhang <sup>1</sup>, Zhengcheng Hou <sup>1</sup>, Mingming Zhang <sup>1,2,\*</sup> , Fangcheng Yan <sup>1</sup>, Jun Gao <sup>1</sup> and Youyou Hu <sup>1</sup> 

<sup>1</sup> School of Science, Jiangsu University of Science and Technology, Zhenjiang 212000, China; zhangfeng23@mails.ucas.ac.cn (F.Z.); 211210501104@stu.just.edu.cn (Z.H.);

221210501114@stu.just.edu.cn (F.Y.); 192210505209@stu.just.edu.cn (J.G.); yyhu@just.edu.cn (Y.H.)

<sup>2</sup> Key Laboratory of Photoelectric Materials and Devices of Zhejiang Province, Ningbo 315211, China

\* Correspondence: zhangmingming@just.edu.cn

**Abstract:** The thermal blooming effect of power-exponent-phase vortex (PEPV) beam propagating in the atmosphere is investigated by employing the multiple phase screen method. The influences of propagation distance, topological charge, power exponent, wind speed, and absorption coefficient on thermal blooming effect are analyzed in detail. The results show that (1) the thermal blooming effect exhibits a significant perturbation on the intensity and phase distribution of PEPV beams, with its influence becoming more pronounced as the propagation distance increases; (2) when the power exponent is fixed at 4, comparing the thermal blooming effect of PEPV beams with different topological charges indicates that a PEPV beam with topological charges of 3 is the most sensitive to thermal blooming; (3) when the topological charge is fixed at 3, the thermal blooming effect decreases with the increase in power exponent; and (4) an increase in wind speed or a decrease in absorption coefficient can reduce the thermal blooming effect. The research results obtained in this article have guiding significance for the application of research into high-energy PEPV beams in the atmosphere.

**Keywords:** power-exponent-phase vortex beam; thermal blooming effect; propagation; phase screen method



**Citation:** Zhang, F.; Hou, Z.; Zhang, M.; Yan, F.; Gao, J.; Hu, Y. Thermal Blooming Effect of Power-Exponent-Phase Vortex Beams Propagating through the Atmosphere. *Photonics* **2023**, *10*, 1343. <https://doi.org/10.3390/photonics10121343>

Received: 10 November 2023

Revised: 2 December 2023

Accepted: 3 December 2023

Published: 5 December 2023



**Copyright:** © 2023 by the authors. Licensee MDPI, Basel, Switzerland. This article is an open access article distributed under the terms and conditions of the Creative Commons Attribution (CC BY) license (<https://creativecommons.org/licenses/by/4.0/>).

## 1. Introduction

High-energy laser beams are frequently indispensable in domains such as optical detection and national defense applications, necessitating their transmission through media like the atmosphere during the application process. In recent years, the propagation of high-energy laser beams in the atmosphere has become a hot research topic [1–3]. Researchers have conducted extensive and in-depth explorations into the behavior and effects of high-energy lasers in the atmosphere, aiming to reveal their physical properties, influencing factors, and potential application prospects.

When a high-power laser beam propagates through the atmosphere, it interacts with the atmosphere and produces a series of linear and non-linear effects. Among these effects, thermal blooming is one of the most significant non-linear effects associated with the propagation of high-power laser beams in the atmosphere. As a high-power laser beam passes through a medium, the medium absorbs some of the beam energy. The absorbed energy, in turn, heats the medium in the atmosphere, which can change the refractive index of the path and lead to a distortion of the beam itself, which is known as the thermal blooming effect [4]. It is a significant challenge in various applications such as laser communication, directed energy weapons, and remote sensing. In recent decades, a growing number of researchers have carried out in-depth research on the thermal blooming effect when a laser beam propagates through the atmosphere. Buser et al. performed numerical simulations of the thermal blooming effect of a Gaussian beam in a uniform wind field using the perturbation method [5]. Mahdieh et al. carried out a two-dimensional simulation of the thermal blooming effect of a ring beam and found that the symmetric dual mode

can be formed when there is no airflow [6]. The Airy beam [7], truncated laser beam [8], Hermite–Gaussian beam [9], array beam [10], Hermite–Gaussian array beam [11], vortex beam [12], and higher-order-mode fiber laser array beam [13] have all been analyzed in detail for their steady-state thermal blooming effects in the atmosphere, and the influences of different parameters have also been studied. Comprehensive studies have indicated that the propagation of a laser beam can be negatively impacted by atmospheric thermal blooming, resulting in detrimental distortions, a dissipation of energy, and a degradation in beam quality. Understanding and mitigating thermal blooming effects are the keys to optimizing the propagation performance of high-power laser beams [14]. In recent years, numerous novel laser modes have emerged, including the power-exponent-phase vortex (PEPV) beam. The PEPV beam is a new type of vortex beam with its phase determined by both the power exponent and the topological charge. One significant advantage of PEPV beams lies in their additional control variable through the power exponent. By adjusting this parameter, we can effectively modulate and manipulate various properties of these beams. This feature opens up new possibilities for applications such as optical communication. In addition, PEPV beams also exhibit promising applications in particle manipulation, integrated optics, quantum safety systems, and information propagation [15–18]. The propagation characteristics of PEPV beams have received widespread attention, such as ABCD systems [19], tight focusing [20,21], oceanic turbulence [22,23], and plasma sheath turbulence [24]. However, research on the propagation performance of high-power PEPV beams in the atmosphere has not yet been conducted.

This paper focuses on a detailed study of the thermal blooming effect of PEPV beams propagating in the atmosphere. In Section 2, the wave equations and hydrodynamic equations for the propagation of PEPV beams in the atmosphere are developed, and the thermal blooming effect in the atmosphere is studied, employing multiple phase screen simulations. In Section 3, the influences of the propagation distance, topological charge, power exponent, wind speed, and absorption coefficient on the thermal blooming effect are investigated in detail during the propagation of PEPV beams in the atmosphere. Moreover, we investigated the combined effects of atmospheric turbulence and thermal blooming on PEPV beams. These contribute to advancing research on the application of PEPV beams.

## 2. Theoretical Model

The Gaussian background PEPV beam in the source plane can be expressed as in [19]:

$$E(r, \varphi) = A_0 \exp(-r^2/(2w^2)) \exp[2il\pi(\varphi/2\pi)^m], \quad (1)$$

where  $(r, \varphi)$  denotes polar coordinates,  $A_0$  and  $w$  are the amplitude and beam waist width of the incident beam, respectively,  $m$  is the power exponent parameter, and  $l$  is the topological charge, such that  $A_0 = \sqrt{P/(\pi w^2)}$ , where  $P$  is the initial power of the PEPV beam.

The phase distribution of PEPV beams with power exponents of 2, 4, 6, and 8 in the source plane for topological charge  $l = 3$  is depicted in Figure 1. A phase singularity with a topological charge of 3 can be observed at the center of the PEPV beam. As  $m$  increases, there is a significant change in phase. It should be pointed out that when  $m = 1$ , the spiral phase factor becomes  $\exp(il\varphi)$ , and the phase distribution of the PEPV beam is the same as that of  $LG_{0,l}$ . Compared to conventional vortex beams, PEPV beams possess an additional control variable through their power exponent  $m$ , which can serve as a carrier of information for applications such as optical communication. Furthermore, due to their distinct phase distribution patterns and controllable parameters, PEPV beams offer enhanced flexibility in shaping light fields for specific purposes.

The laser intensity affected by atmospheric absorption is denoted by

$$I = |E|^2 \exp(-\alpha z), \quad (2)$$

where  $\alpha$  is the atmospheric absorption coefficient,  $z$  is the propagation distance, and  $I$  is the laser intensity.

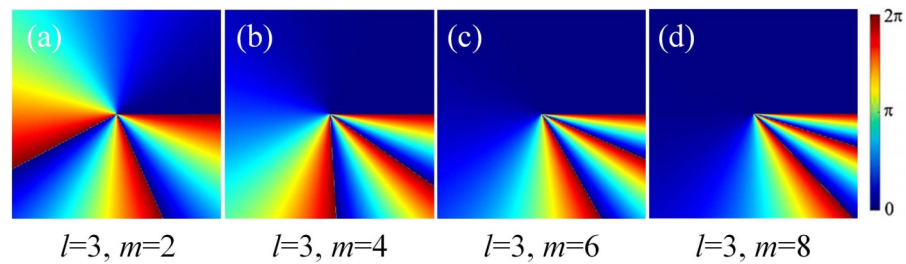


**Figure 1.** Phase distribution of PEPV beams in the source plane. (a)  $l = 3, m = 2$ ; (b)  $l = 3, m = 4$ ; (c)  $l = 3, m = 6$ ; (d)  $l = 3, m = 8$ .

It has been shown that the thermal blooming effect is mainly described by the paraxial scalar wave equation and fluid mechanics equations when the PEPV beam propagates in the atmosphere. Assuming that the beam propagates along the  $z$ -axis, Maxwell’s paraxial wave equation is expressed as in [25]:

$$2ik \frac{\partial E}{\partial z} = \nabla_{\perp}^2 E + k^2 \left( \frac{n^2}{n_0^2} - 1 \right) E, \tag{3}$$

where  $\nabla_{\perp}^2 = \frac{\partial^2}{\partial x^2} + \frac{\partial^2}{\partial y^2}$  is the Laplace operator,  $n$  is the refractive index in the atmosphere,  $n_0$  is the refractive index at rest in the atmosphere, usually set to 1.000313,  $k$  is the wave number associated with the wavelength  $\lambda$ , and  $k = 2\pi/\lambda$ . Further, under isobaric approximation, combined with atmospheric absorption, the hydrodynamic equation can be obtained as in [25]:

$$\frac{\partial \rho}{\partial t} + v \nabla \rho = - \frac{(\gamma - 1)}{c_s^2} \alpha I, \tag{4}$$

where  $\gamma$  is the specific heat ratio,  $c_s$  is the speed of sound,  $v$  is the atmospheric fluid velocity, and  $\rho$  is the change in the density of the atmosphere. Further, based on the relationship between the atmospheric refractive index and density, one obtains the following [12,26]:

$$\frac{n^2}{n_0^2} - 1 \approx 2(n_0 - 1) \frac{\rho}{\rho_0}, \tag{5}$$

where  $\rho_0$  is the atmospheric density in the absence of perturbations. Using the Taylor series and the second-order accuracy of the symmetric splitting operator, at propagation distance  $z^{n+1} = z^n + \Delta z$ , from Equation (3), it follows that [25]

$$E^{(n+1)} = \exp\left(-\frac{i}{4k} \Delta z \nabla_{\perp}^2\right) \exp\left[-\frac{ik}{2} \int_{z^n}^{z^n + \Delta z} \left(\frac{n^2}{n_0^2} - 1\right) dz\right] \exp\left(-\frac{i}{4k} \Delta z \nabla_{\perp}^2\right) E^n. \tag{6}$$

It is shown that the propagation field from  $z^n$  to  $z^{n+1}$  can be divided into three parts: the first and the last parts represent free propagation in a vacuum over a distance of  $\Delta z/2$ , and the middle part is attributed to changes in the refractive index caused by thermal blooming. The entire propagation process can be simulated using the multiple phase screen method. The PEPV beam described in Equation (1) is used as the initial light field and equally spaced phase screens are placed along the  $z$ -axis to simulate the effect of atmospheric thermal blooming. The distance between adjacent phase screens is  $\Delta z$ , with the first phase screen positioned at a distance of  $\Delta z/2$ . Consequently, the PEPV beam initially propagates through the free space for  $\Delta z/2$ , encounters a phase screen, and then freely propagates for another  $\Delta z/2$  before reaching the first receiving screen. The light field at  $\Delta z$  is represented as

$$E_1(x, y) = F^{-1} \left\{ F \left\{ F^{-1} \left\{ F \left[ E_0(x, y) \right] \cdot U(k_x, k_y) \right\} \exp[i\varphi(x, y)] \right\} \cdot U(k_x, k_y) \right\}, \tag{7}$$

where the  $F$  and  $F^{-1}$  represent the Fourier transform and Fourier inverse transform, respectively,  $E_0(x,y)$  represents the initial light field of the PEPV beam,  $\varphi(x,y)$  is the phase distribution of the virtual thermal blooming distortion phase screen,  $U(k_x,k_y)$  represents the transfer function in the spatial frequency domain, and  $k_x$  and  $k_y$  are the spatial frequency components in the  $x$ - and  $y$ -axis directions, respectively. In Equation (7), the Fourier and inverse Fourier transforms are applied twice each. Initially, the initial light field underwent a Fourier transform to be converted into the frequency domain. It was then multiplied by the transfer function corresponding to  $\Delta z/2$  distance and subsequently subjected to an inverse Fourier transform to obtain the distribution of the light field after free transmission over  $\Delta z/2$  distance. Subsequently, the light field was multiplied by the thermal blooming phase factor, followed by another round of Fourier transform and inverse Fourier transform to acquire the propagated light field up to  $\Delta z$ .

By repeating the above calculation process, we could obtain the distribution of the light field at different distances.

### 3. Results and Discussion

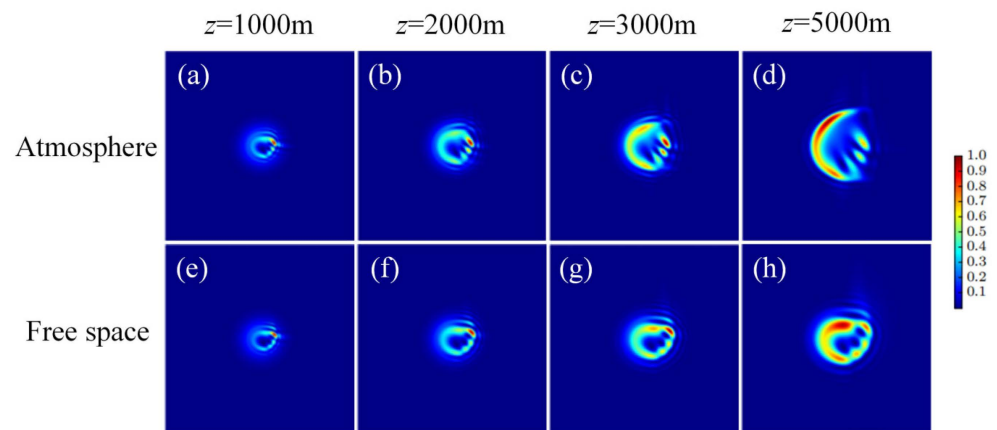
The thermal blooming effect of PEPV beams propagating through the atmosphere is influenced by various factors, such as propagation distance, topological charge, power exponent, transverse wind speed, and absorption coefficient. Here, we used the multiple phase screen method for simulation analysis. Since large or small grid spacing would affect the accuracy of the numerical calculation and cause errors in the calculation results, the parameters were selected according to Nyquist’s theorem and set to spacing of 200 m, a grid number of  $512 \times 512$ , and a screen width of  $8w$ , where  $w$  is the waist radius. The simulation selection parameters were as follows:  $\gamma = 1.4$ , sound velocity  $c_s = 340$  m/s, air density  $\rho_0 = 1.3025$  kg/m<sup>3</sup>, wavelength  $\lambda = 1064$  nm, waist radius  $w = 0.1$  m, initial power  $P = 20$  kW, absorption coefficient  $\alpha = 6.5 \times 10^{-5}$  m<sup>-1</sup>, wind speed  $v = 6$  m/s along the  $x$ -axis, propagation distance  $z = 3$  km, and distance separation  $\Delta z = 200$  m.

The intensity distribution of a PEPV beam will change considerably due to the thermal blooming effect. Here, we describe the beam quality according to a change in spot centroid position. Since the wind direction is along the  $x$ -axis, we only consider the  $x$ -axis component of the centroid position here, whose mathematical expression is [12]

$$\bar{x} = \frac{\int_{-\infty}^{\infty} \int_{-\infty}^{\infty} xI(x,y,z)dx dy}{\int_{-\infty}^{\infty} \int_{-\infty}^{\infty} I(x,y,z)dx dy} \tag{8}$$

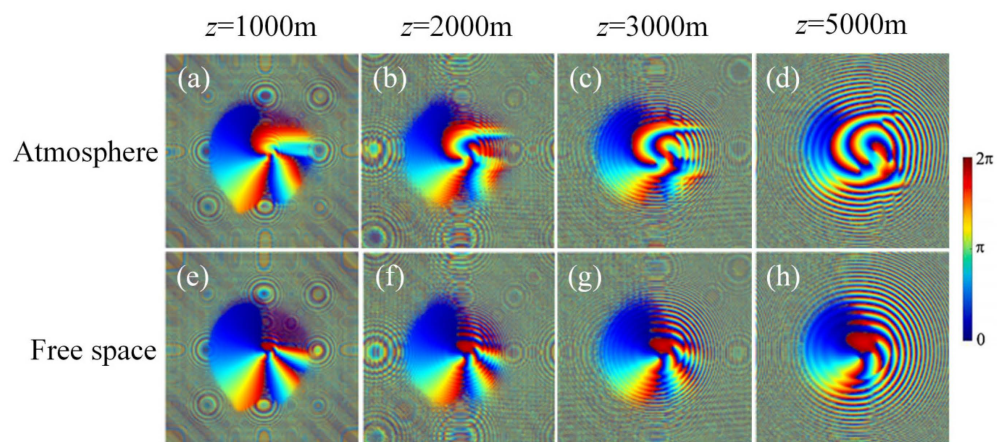
#### 3.1. Propagation Distance

Figure 2 shows the intensity distribution of the PEPV beam at 1000 m, 2000 m, 3000 m, and 5000 m, where the topological charge of the PEPV beam is selected as 3 and the power exponent is 4. To accurately study the effect of thermal blooming, the intensity distribution of the PEPV beam propagating in free space is also simulated. In free space, the number of central dark spots consistent with the topological charge can be clearly observed, and the profile of the PEPV beam bears resemblance to that of a clenched fist. When a PEPV beam propagates in the atmosphere, the intensity distribution of the PEPV beam within a propagation distance of 2000 m is roughly the same as that of free propagation, with both showing a fist-like shape. But, as the distance increases, the light spot gradually expands, the size increases, and the right-hand opening becomes larger, which is significantly different from the light intensity distribution in the absence of thermal blooming. The reason for this is that as the distance  $z$  increases, the energy absorbed by the atmosphere increases, and the impact of thermal blooming on the propagation of laser beams will be enhanced.



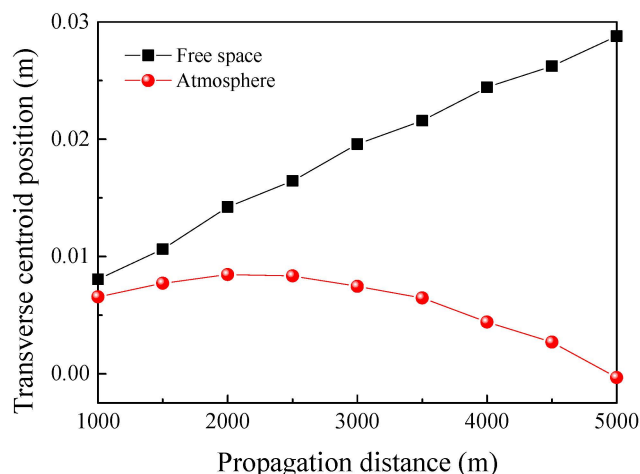
**Figure 2.** Intensity distribution of a PEPV beam at different propagation distances. In the atmosphere: (a)  $z = 1000$  m, (b)  $z = 2000$  m, (c)  $z = 3000$  m, (d)  $z = 5000$  m; in free space: (e)  $z = 1000$  m, (f)  $z = 2000$  m, (g)  $z = 3000$  m, (h)  $z = 5000$  m.

Figure 3 shows the phase distribution corresponding to Figure 2. It can be found that a phase singularity with topological charge  $l = 3$  breaks up into three phase singularities with topological charge  $l = 1$  during propagation, and the spacing between the phase singularities gradually increases as the propagation distance increases. According to Figure 3, it can be observed that due to the thermal blooming effect, the phase distribution changes with an increasing propagation distance, and the distortion of the phase distribution becomes significantly enhanced.



**Figure 3.** Phase distribution of a PEPV beam at different propagation distances. In the atmosphere: (a)  $z = 1000$  m, (b)  $z = 2000$  m, (c)  $z = 3000$  m, (d)  $z = 5000$  m; in free space: (e)  $z = 1000$  m, (f)  $z = 2000$  m, (g)  $z = 3000$  m, (h)  $z = 5000$  m.

Due to its unique phase structure, the centroid position of a PEPV beam does not remain constant during free space propagation, as shown in Figure 4. Figure 4 shows the transverse centroid positions of a PEPV beam propagating through free space and the atmosphere, respectively. In free space, the transverse centroid position of the light spot gradually increases with the increase in distance  $z$ . When the PEPV beam propagates in the atmosphere, the transverse centroid position also changes due to the thermal blooming effect. A comparison shows that as propagation distance increases, there is a growing disparity between centroid positions for these two cases, indicating an escalating influence of thermal blooming on the propagation of laser beams.



**Figure 4.** Variation in the transverse centroid position with propagation distance.

### 3.2. The Topological Charge and Power Exponent

The topological charge  $l$  and power exponent  $m$  are important parameters for PEPV beams. Here, we focus on analyzing the effects of the power exponent and the topological charge numbers on the thermal blooming effect during the propagation of PEPV beams. Figure 5 shows the intensity distribution of PEPV beams with different topological charges and power exponents propagating in the atmosphere at a propagation distance of 3 km. In order to clarify the impact of thermal blooming on the beam, the intensity distribution of the PEPV beam propagating in free space is also simulated, as shown in Figure 6. The number of dark cores near the middle of the beam consistent with the topological charge  $l$  can be clearly observed in both Figures 5 and 6. And, it can be found that at a certain power exponent, as the topological charge number increases, the spot area also becomes larger. Compared to Figure 6, it can be observed from Figure 5 that due to the thermal blooming effect, the shape of the light spot underwent significant changes, and the size of the light spot significantly increased.

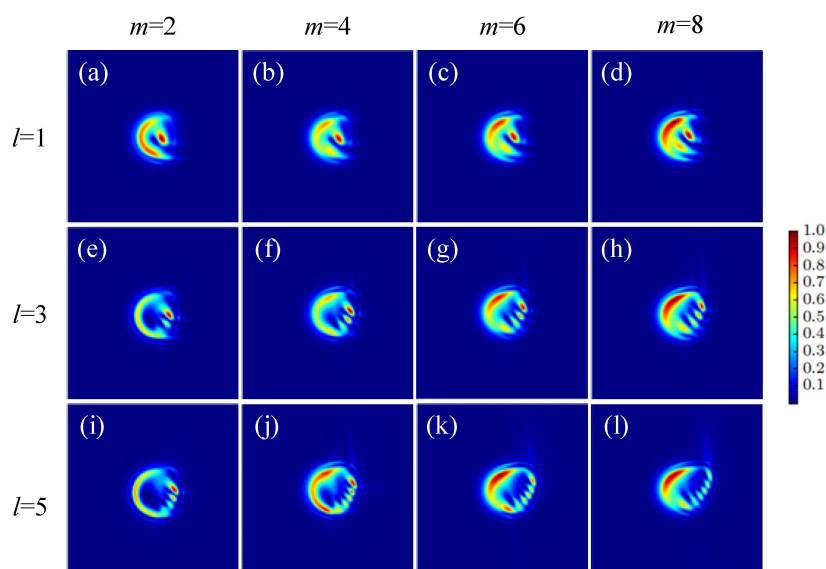


**Figure 5.** Intensity distribution of PEPV beams with different topological charges and power exponents propagating in the atmosphere at a propagation distance of 3 km. (a)  $l = 1, m = 2$ ; (b)  $l = 1, m = 4$ ; (c)  $l = 1, m = 6$ ; (d)  $l = 1, m = 8$ ; (e)  $l = 3, m = 2$ ; (f)  $l = 3, m = 4$ ; (g)  $l = 3, m = 6$ ; (h)  $l = 3, m = 8$ ; (i)  $l = 5, m = 2$ ; (j)  $l = 5, m = 4$ ; (k)  $l = 5, m = 6$ ; (l)  $l = 5, m = 8$ .

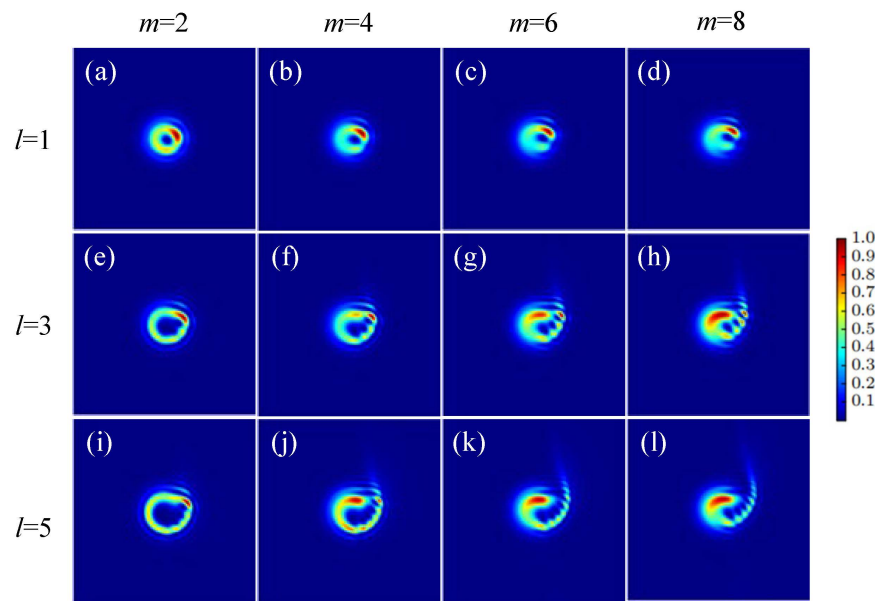


**Figure 6.** Intensity distribution of PEPV beams with different topological charges and power exponents propagating in free space at a propagation distance of 3 km. (a)  $l = 1, m = 2$ ; (b)  $l = 1, m = 4$ ; (c)  $l = 1, m = 6$ ; (d)  $l = 1, m = 8$ ; (e)  $l = 3, m = 2$ ; (f)  $l = 3, m = 4$ ; (g)  $l = 3, m = 6$ ; (h)  $l = 3, m = 8$ ; (i)  $l = 5, m = 2$ ; (j)  $l = 5, m = 4$ ; (k)  $l = 5, m = 6$ ; (l)  $l = 5, m = 8$ .

### 3.3. Wind Speed

The intensity distribution of a PEPV beam with a topological charge of 3 and a power exponent of 4 under varying wind speeds is depicted in Figure 7. As the wind speed increases, the distortion of the light spot decreases, indicating that the thermal blooming effect is weakening. This result suggests that higher wind speeds facilitate rapid dissipation of energy absorbed by the atmosphere during the propagation of PEPV beams, resulting in reduced temperature fluctuations along the atmospheric path and consequently diminished refractive index variations. Ultimately, this leads to a mitigation of thermal blooming and an improvement in beam quality.

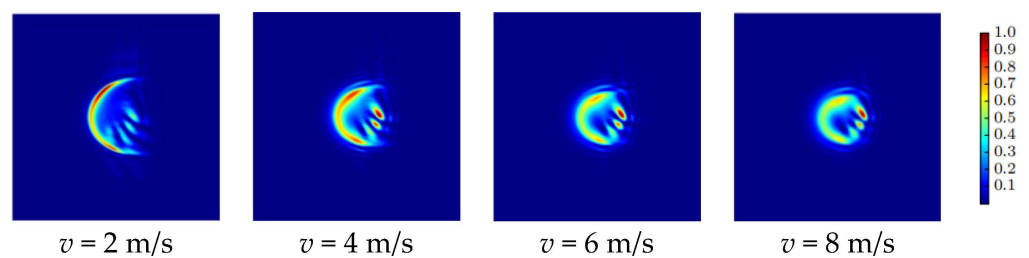


**Figure 7.** Intensity distribution of a PEPV beam with  $l = 3$  and  $m = 4$  propagating in the atmosphere for different wind speeds.

Due to the fact that the centroid position of the PEPV beam during free space propagation is not at the origin position, in order to accurately describe the changes in centroid position under the thermal blooming effect, we introduce the concept of a relative transverse centroid position. The relative transverse centroid position is defined as the difference between the transverse centroid positions of the light spot affected and unaffected by the thermal blooming, and is formulated as follows:

$$\Delta \bar{x} = |\bar{x} - \bar{x}_0|, \tag{9}$$

where  $\bar{x}_0$  is the transverse centroid position of the PEPV beam propagating in free space.

Variation in the relative transverse centroid position of PEPV beams with different topological charges (see Figure 8a) and power exponents (see Figure 8b) as a function of wind speed is depicted in Figure 8. As the wind speed increases, the relative transverse centroid positions of the PEPV beams gradually decrease. As shown in the inset of Figure 8a, with a power exponent of 4 and a wind speed of 3 m/s, the relative transverse centroid position first increases and then decreases as the topological charge number increases. When the topological charge number is 3, the relative transverse centroid position reaches its maximum value, indicating that thermal blooming has its greatest impact on the light spot at this point. These findings suggest that selecting an appropriate topological charge can mitigate the impact of thermal blooming on the propagation of PEPV beams. Moreover, as illustrated in Figure 8b, when considering a fixed topological charge value of 3, an increase in the power exponent results in a smaller relative transverse centroid position. This implies that higher power exponents help alleviate the thermal blooming effect. Therefore, the impact of thermal blooming on the propagation of PEPV beams can be effectively mitigated by carefully selecting the appropriate topological charge and power exponent.

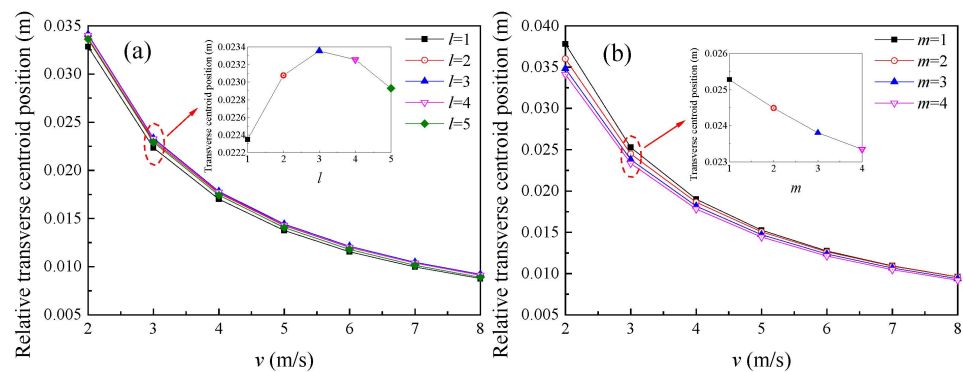


**Figure 8.** Variation in the relative transverse centroid position of a PEPV beam with wind speed. (a) Power exponent  $m = 4$ , topological charge  $l = 1, 2, 3, 4, 5$ ; (b) topological charge  $l = 3$ , power exponent  $m = 1, 2, 3, 4$ .

### 3.4. Absorption Coefficient

The absorption coefficient is a crucial factor influencing the intensity of the thermal blooming effect. As illustrated in Figure 9, the intensity distribution of PEPV beams with  $l = 3$  and  $m = 4$  at a propagation distance of 3 km is presented under different absorption coefficients. It was found that an increase in the absorption coefficient led to heightened intensity distortion and intensified thermal blooming effects. This was primarily due to an increase in laser energy absorbed by the atmosphere, resulting in a stronger interaction between the PEPV beam and the atmospheric conditions along its propagation path. This means that an increase in the absorption coefficient will cause more heat to reside on the propagation path of the laser beam, increasing the change in the refractive index of the air, enhancing the thermal blooming effect, and reducing the laser energy reaching the target point. From Figure 10, it can be seen that as the absorption coefficient increases, the relative transverse centroid position of the PEPV beam shows an upward trend, indicating a significant enhancement in the thermal blooming effect. PEPV beams with different topological charges and power exponents exhibit the same trend of change. Under the same absorption coefficient, the influence of topological charge and power exponent on the thermal blooming effect is roughly the same as that observed in the wind speed module, further verifying the influence of topological charge and power exponent on the thermal blooming effect. By carefully selecting the topological charge and power exponent, which determine the spatial structure of PEPV beams, we can optimize their propagation characteristics.

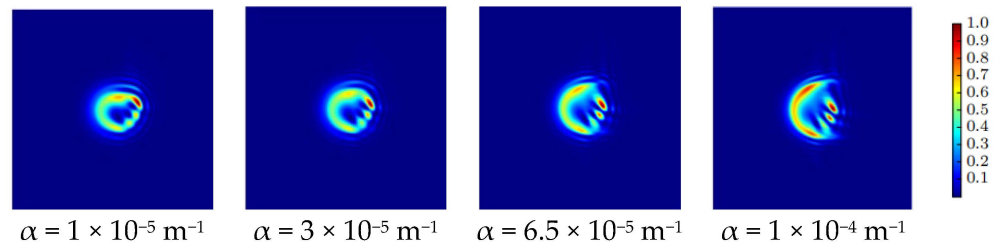


**Figure 9.** Intensity distribution of a PEPV beam propagating in the atmosphere under different absorption coefficients.

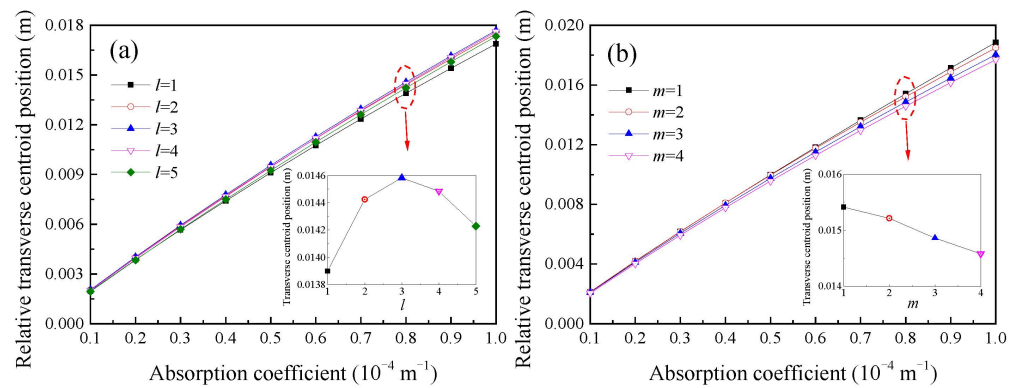


**Figure 10.** Variation in relative transverse centroid position of a PEPV beam with an absorption coefficient. (a) Power exponent  $m = 4$ , topological charge  $l = 1, 2, 3, 4, 5$ ; (b) topological charge  $l = 3$ , power exponent  $m = 1, 2, 3, 4$ .

### 3.5. Atmospheric Turbulence

In our previous analysis, we did not take into account the influence of atmospheric turbulence. However, it is crucial to consider atmospheric turbulence as one of the significant factors that affect the propagation of laser beams. Atmospheric turbulence refers to the random fluctuations in air density and temperature that can distort and scatter light beams passing through it. Hence, in this section, we will concurrently examine the combined impact of turbulence and thermal blooming on the propagation of PEPV beams. Equation (7) only considers the influence of thermal blooming through the phase factor  $\exp[i\varphi(x,y)]$ . Here, we need to incorporate the phase disturbance  $\psi(x,y)$  caused by turbulence. After comprehensive consideration, we modified the phase factor  $\exp[i\varphi(x,y)]$  to  $\exp[i\varphi(x,y) + i\psi(x,y)]$ . This modification allowed us to account for both thermal blooming and turbulent effects simultaneously. To establish a turbulent phase screen for our study, we employed the power spectrum inversion method [27]. The simulation selection parameters were as follows:  $w = 0.1$  m,  $P = 20$  kW,  $\alpha = 6.5 \times 10^{-5} \text{ m}^{-1}$ ,  $v = 6$  m/s,  $\Delta z = 200$  m, and turbulence strength  $C_n^2 = 2 \times 10^{-16} \text{ m}^{-2/3}$ . Furthermore, the standard deviation of the relative transverse centroid position was introduced for analyzing the combined effects of turbulence and thermal blooming on PEPV beams. Its expression is as follows:

$$\sigma = \sqrt{2\langle \Delta \bar{x}^2 \rangle} \tag{10}$$

where  $\langle \rangle$  indicates ensemble average.

Variation in the standard deviation of the relative transverse centroid position of a PEPV beam with respect to topological charge and power exponent at propagation distances of 1000 m, 2000 m, and 3000 m is illustrated in Figure 11. When the power exponent is set to 4, it can be observed from Figure 11a that an increase in topological charge does not result in a significant change in the standard deviation of the relative transverse centroid position. However, as the propagation distance increases, there is a notable increase in the standard deviation of the relative transverse centroid position.

This suggests that propagation distance primarily influences relative transverse centroid position while topological charges play a minor role. Similarly, as shown in Figure 11b, when the topological charge is 3, comparing the standard deviation of the relative transverse centroid position under different power exponents, it can be found that as the power exponent gradually increases, the standard deviation of the relative centroid position remains basically unchanged. In Figure 11b, as the propagation distance increases, the standard deviation of the relative transverse centroid position also significantly increases. Therefore, it can be concluded that in a turbulent atmosphere, the propagation distance has a significant impact on the PEPV beams, while the mode order has little effect.

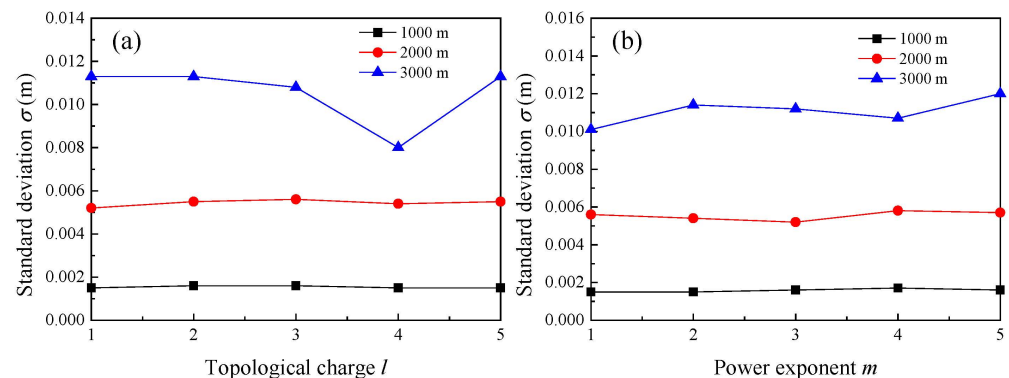


**Figure 11.** The standard deviation of the relative transverse centroid position of a PEPV beam with different topological charges and power exponents. (a) Power exponent  $m = 4$ , topological charge  $l = 1, 2, 3, 4, 5$ ; (b) topological charge  $l = 3$ , power exponent  $m = 1, 2, 3, 4, 5$ .

By incorporating atmospheric turbulence into our analysis and modifying our model accordingly, we can obtain a more precise understanding of the propagation of PEPV beams in real-world conditions.

#### 4. Conclusions

In this article, a detailed analysis has been conducted on the impact of propagation distance, topological charge, power exponent, wind speed, and absorption coefficient on thermal blooming using the multiple phase screen method. Numerical simulations showed that as the propagation distance increased, spot expansion and distortion became more severe. Increasing wind speed dissipates heat in the propagation path of laser beams, reducing thermal blooming effects. Higher absorption coefficients cause more heat to reside in the path, increasing thermal blooming and decreasing laser energy at target points. The relative transverse centroid position of a PEPV beam with  $m = 4$  initially increases and then decreases with increasing topological charge. It reaches its maximum value when  $l = 3$ . Increasing the power exponent, while keeping the topological charge fixed, results in a smaller relative transverse centroid position. Therefore, adjusting both the topological charge and power exponent can reduce the influence of thermal blooming on the propagation of PEPV beams. The research results have important guiding significance for the effective application of PEPV beams in fields such as optical communication.

**Author Contributions:** Conceptualization, F.Z. and M.Z.; methodology, M.Z.; software, F.Z. and Z.H.; validation, F.Z., Z.H. and F.Y.; formal analysis, Y.H.; investigation, J.G.; resources, M.Z.; data curation, F.Z.; writing—original draft preparation, F.Z. and M.Z.; writing—review and editing, M.Z., Z.H., F.Y. and J.G.; supervision, Y.H.; project administration and funding acquisition, M.Z. All authors have read and agreed to the published version of the manuscript.

**Funding:** This research was funded by General Project of Natural Science research in Colleges and Universities of Jiangsu Province (grant no. 20KJB14008), the Opening Project of the Key Laboratory of Photoelectric Materials and Devices of Zhejiang Province (grant no. KLPMD2105), and the Jiangsu Province Industry University Research Cooperation Project (grant no. BY2020680).

**Institutional Review Board Statement:** Not applicable.

**Informed Consent Statement:** Not applicable.

**Data Availability Statement:** The data underlying the results presented in this paper are not publicly available at this time but may be obtained from the authors upon reasonable request.

**Conflicts of Interest:** The authors declare no conflict of interest.

## References

1. Van Zandt, N.R.; Fiorino, S.T.; Keefer, K.J. Enhanced, fast-running scaling law model of thermal blooming and turbulence effects on high energy. *Opt. Express* **2013**, *21*, 14789–14798. [[CrossRef](#)] [[PubMed](#)]
2. Shlenov, S.A.; Vasiltsov, V.V.; Kandidov, V.P. Energy parameters of CO<sub>2</sub> laser radiation focused in a turbulent atmosphere under wind-dominated thermal blooming. *Atmos. Ocean. Opt.* **2016**, *29*, 324–330. [[CrossRef](#)]
3. Zhang, Q.; Hu, Q.; Wang, H.; Hu, M.; Xu, X.; Wu, J.; Hu, L. High-precision calculation and experiments on the thermal blooming of high-energy lasers. *Opt. Express* **2023**, *31*, 25900–25914. [[CrossRef](#)]
4. Smith, D.C. High-power laser propagation: Thermal blooming. *Proc. IEEE* **1977**, *65*, 1679–1714. [[CrossRef](#)]
5. Buser, R.G.; Rohde, R.S.; Berger, P.J.; Gebhardt, F.G.; Smith, D.C. Transient thermal blooming of single and multiple short laser pulses. *Appl. Opt.* **1975**, *14*, 2740–2746. [[CrossRef](#)] [[PubMed](#)]
6. Mahdiah, M.; Lotfi, B. Two-dimensional-simulation of thermal blooming effects in ring pattern laser beams. *Opt. Eng.* **2005**, *44*, 096001. [[CrossRef](#)]
7. Ji, X.; Eyyuboğlu, H.T.; Ji, G.; Jia, X. Propagation of an Airy beam through the atmosphere. *Opt. Express* **2013**, *21*, 2154–2164. [[CrossRef](#)]
8. Li, X.; Ji, X. Effect of thermal blooming on the beam quality of truncated laser beams. *Optik* **2016**, *127*, 8350–8356. [[CrossRef](#)]
9. Ding, Z.; Li, X.; Cao, J.; Ji, X. Thermal blooming effect of Hermite-Gaussian beams propagating through the atmosphere. *J. Opt. Soc. Am. A* **2019**, *36*, 1152–1160. [[CrossRef](#)] [[PubMed](#)]
10. Li, X.; Cao, J.; Ding, Z.; Ji, X. Influence of fill factors on the thermal blooming of array laser beams in the air. *Optik* **2019**, *182*, 314–323. [[CrossRef](#)]
11. Ding, Z.; Li, X.; Cao, J.; Ji, X. Influence of thermal blooming on the beam quality of an array of Hermite-Gaussian beams propagating in the atmosphere. *Appl. Opt.* **2020**, *59*, 10944–10952. [[CrossRef](#)]
12. Zhao, L.; Wang, J.; Guo, M.; Xu, X.; Qian, X.; Zhu, W.; Li, J. Steady-state thermal blooming effect of vortex beam propagation through the atmosphere. *Opt. Laser Technol.* **2021**, *139*, 106982. [[CrossRef](#)]
13. Zhang, Y.; Hou, T.; Deng, Y.; Ma, P.; Su, R.; Zhou, P. Effect of thermal blooming on the higher-order mode fiber laser array propagation through the atmosphere. *Front. Phys.* **2022**, *10*, 880436. [[CrossRef](#)]
14. Zhong, Z.; Qiu, D.; Zhang, B. Mitigating thermal blooming effect of seawater using self-rotating beam. *Opt. Commun.* **2023**, *531*, 129215. [[CrossRef](#)]
15. Pei, Z.; Huang, S.; Chen, Y.; Yan, C. Comparison of microparticle manipulating characteristics of canonical vortex beam and power-exponent-phase vortex beam. *J. Mod. Optic.* **2021**, *68*, 224–232. [[CrossRef](#)]
16. Wu, Z.; Zhao, J.; Dou, J.; Liu, J.; Jing, Q.; Li, B.; Hu, Y. Optical trapping of multiple particles based on a rotationally-symmetric power-exponent-phase vortex beam. *Opt. Express* **2022**, *30*, 42892–42901. [[CrossRef](#)]
17. Fan, C.; Liu, Y.; Wang, X.; Chen, Z.; Pu, J. Trapping two types of particles by using a tightly focused radially polarized power-exponent-phase vortex beam. *J. Opt. Soc. Am. A* **2018**, *35*, 903–907. [[CrossRef](#)]
18. Liu, X.; Wang, M.; Guo, L.; Cheng, S.; Tao, S. Measuring the photonic topological charge of power-exponent-phase vortex beam via cross phase. *Appl. Phys. Lett.* **2023**, *123*, 034104. [[CrossRef](#)]
19. Lao, G.; Zhang, Z.; Zhao, D. Propagation of the power-exponent-phase vortex beam in paraxial ABCD system. *Opt. Express* **2016**, *24*, 18082–18094. [[CrossRef](#)]
20. Chen, K.; Ma, Z.-Y.; Hu, Y.-Y. Tightly focused properties of a partially coherent radially polarized power-exponent-phase vortex beam. *Chin. Phys. B* **2023**, *32*, 024208. [[CrossRef](#)]
21. Chen, K.; Ma, Z.; Zhang, M.; Dou, J.; Hu, Y. The tight-focusing properties of radially polarized symmetrical power-exponent-phase vortex beam. *J. Opt.* **2022**, *24*, 055602. [[CrossRef](#)]
22. Pan, Y.; Zhao, M.; Zhang, M.; Dou, J.; Zhao, J.; Li, B.; Hu, Y. Propagation properties of rotationally-symmetric power-exponent-phase vortex beam through oceanic turbulence. *Opt. Laser Technol.* **2023**, *159*, 109024. [[CrossRef](#)]
23. Wang, J.; Wang, X.; Peng, Q.; Zhao, S. Propagation characteristics of autofocusing Airy beam with power exponential phase vortex in weak anisotropic oceanic turbulence. *J. Mod. Optic.* **2021**, *68*, 1059–1065. [[CrossRef](#)]
24. Chen, C.; Chen, W.; Deng, Q.; Yang, L.; Deng, W.; Zeng, M.; Ma, Q.; Huang, Z. Study on propagation properties of orbital angular momentum modes in plasma sheath turbulence for power-exponent-phase Airy beams. *IEEE Antenn. Wirel. Propag. Lett.* **2023**, *22*, 94–98. [[CrossRef](#)]
25. Fleck Jr, J.A.; Morris, J.R.; Feit, M.D. Time-dependent propagation of high energy laser beams through the atmosphere. *Appl. Phys.* **1976**, *10*, 129–160. [[CrossRef](#)]

26. Zhang, Y.; Hou, T.; Chang, H.; Su, R.; Ma, P.; Zhou, P. Thermal blooming effect and the scaling laws of partial spatially coherent beam array propagating through the atmosphere. *Results Phys.* **2021**, *26*, 104444. [[CrossRef](#)]
27. Yong, K.; Yan, J.; Huang, S.; Zhang, R. Propagation characteristics of optical vortex pulse in atmospheric turbulence. *Optik* **2019**, *180*, 27–33. [[CrossRef](#)]

**Disclaimer/Publisher's Note:** The statements, opinions and data contained in all publications are solely those of the individual author(s) and contributor(s) and not of MDPI and/or the editor(s). MDPI and/or the editor(s) disclaim responsibility for any injury to people or property resulting from any ideas, methods, instructions or products referred to in the content.